University of New Hampshire

University of New Hampshire Scholars' Repository

Physics Scholarship   Physics

7-11-2008

Inherent length-scales of periodic solar wind number density structures

N. M. Viall

L. Kepko

Harlan E. Spence
Boston University, harlan.spence@unh.edu

Recommended Citation

Viall, N. M., L. Kepko, and H. E. Spence (2008), Inherent length-scales of periodic solar wind number density structures, J. Geophys. Res., 113, A07101, doi:10.1029/2007JA012881.

Inherent length-scales of periodic solar wind number density structures

N. M. Viall,[1] L. Kepko,[2] and H. E. Spence[1]

[1]   We present an analysis of the radial length-scales of periodic solar wind number density structures. We converted 11 years (1995–2005) of solar wind number density data into radial length series segments and Fourier analyzed them to identify all spectral peaks with radial wavelengths between 72 (116) and 900 (900) Mm for slow (fast) wind intervals. Our window length for the spectral analysis was 9072 Mm, approximately equivalent to 7 (4) h of data for the slow (fast) solar wind. We required that spectral peaks pass both an amplitude test and a harmonic F-test at the 95% confidence level simultaneously. From the occurrence distributions of these spectral peaks for slow and fast wind, we find that periodic number density structures occur more often at certain radial length-scales than at others, and are consistently observed within each speed range over most of the 11-year interval. For the slow wind, those length-scales are L $\sim$ 73, 120, 136, and 180 Mm. For the fast wind, those length-scales are L $\sim$ 187, 270 and 400 Mm. The results argue for the existence of inherent radial length-scales in the solar wind number density.

Citation: Viall, N. M., L. Kepko, and H. E. Spence (2008), Inherent length-scales of periodic solar wind number density structures, *J. Geophys. Res.*, *113*, A07101, doi:10.1029/2007JA012881.

1.   Introduction

[2]   Recent studies have revealed the existence of highly periodic number density variations in the solar wind at 1 AU [*Kepko et al.*, 2002; *Stephenson and Walker*, 2002; *Kepko and Spence*, 2003]. These event studies analyzed the observed frequencies of the solar wind number density structures in order to relate them to observed magnetospheric oscillations. *Kepko and Spence* [2003] argued that the observed oscillations were not propagating waves, but were periodic number density structures frozen in the solar wind. The structures convect with the ambient solar wind, and therefore appear at discrete frequencies in the spacecraft's reference frame. Using this argument, they converted the frequencies observed in their event studies into equivalent periodic radial length-scales and found that those frequencies most often corresponded to radial length-scales (L) of $\sim$23, 30, 45, and 80–100 R_E (150, 200, 300, and 500–600 Mm).

[3]   The aforementioned studies presented only a few events and did not determine whether periodic number density structures in the solar wind were recurrent at certain radial length-scales. Theoretically, as a consequence of turbulence, one would not expect to find a particular set of recurrent periodic length-scales in the solar wind [*Bruno and Carbone*, 2005]. In the presence of turbulence, the average solar wind spectra in the 10–1000 Mm range should follow a power law, with no spectral enhancements at discrete wavelengths. Spectra calculated over short segments may exhibit significant spectral power at discrete wavelengths but, in a statistical sense, one would not expect significant spectral peaks at any particular wavelength to occur more often than at other wavelengths. In other words, there should not exist sets of wavelengths that are more likely to be observed than others. Because turbulent fluctuations may cause significant spectral enhancements in short segments, event studies alone cannot establish whether particular discrete radial wavelengths are inherent to solar wind number density structures.

[4]   In this paper, we present an analysis of the relative occurrence rate of statistically significant periodic solar wind number density structures. We explore radial wavelengths between L = 72–900 Mm identified in eleven years of solar wind data, analyzing separately the slow and fast wind. We answer the question of whether periodic solar wind number density structures are more likely to occur at particular, discrete, radial length-scales. We first describe data preparation and analysis methodology. We use the techniques of *Thomson* [1982] and *Mann and Lees* [1996] to determine the relative occurrence rate of statistically significant periodic solar wind number density structures in 9072 Mm long intervals, equivalent to approximately 7 (4) h for the slow (fast) solar wind data. The results show that the periodic solar wind number density structures occur more often at particular radial length-scales, with some

_____

[1]Center for Space Physics, Boston University, Boston, Massachusetts, USA.
[2]Space Science Center, University of New Hampshire, Durham, New Hampshire, USA.
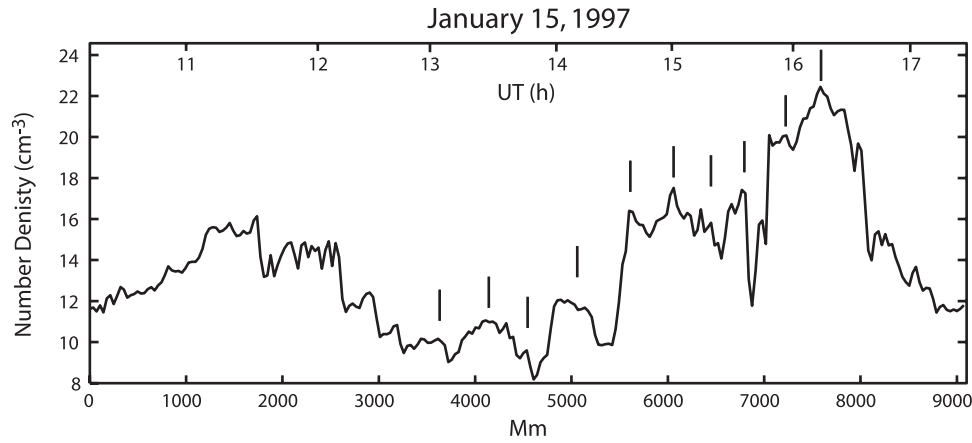
Figure 1. Solar wind number density data for 15 January 1997. Bottom x axis is in radial-length scale steps, top x axis shows the corresponding UT. Tick marks indicate a clear $\sim$400 Mm periodicity.

consistency both over the 11-year interval and between the fast and slow wind.

2. Methods

[5] We examined 11 years (1995–2005) of solar wind number density measurements from the Solar Wind Experiment (SWE) on the Wind spacecraft [*Ogilvie et al.*, 1995]. We first converted all 11 years of number density data from a time series into a radial length-scale series by multiplying each time step (Δt) by the radial velocity (V_x) observed at that time step. We interpolated the entire 11-year length-scale series to a common 35.4 Mm length step for slow solar wind and to a 56.7 Mm length step for the fast solar wind. We defined "fast" segments as those with an average radial speed $\geq$550 km/s and "slow" segments as those with an average radial speed <550 km/s. We chose the aforementioned sampling rates to maximize the sampling resolution, while minimizing the amount of interpolation for each speed range; they are equivalent to approximately the median solar wind speeds in each range at one AU multiplied by the instrument sampling rate (90s). We find that other similar sampling rates for a given speed range do not significantly change the results presented here.

[6] We analyzed overlapping 9072-Mm-long segments (hereinafter referred to as "segments") equivalent to approximately 7 (4) h for the slow (fast) wind, shifting each segment by 252 Mm. Data with a quality flag value indicating poor quality were removed. To minimize the inclusion of spurious spectral peaks, we further required that each segment pass multiple criteria to be included in our analysis. The first requirement was that the Wind spacecraft was located at $X > 50\ R_E$ to ensure that we included only undisturbed, upstream solar wind; the distance criterion eliminated intervals compromised by magnetospheric and foreshock encounters. The second requirement was that the percent of flagged or missing data within a segment could not exceed 10% if it was randomly distributed throughout the segment, and could not exceed 3% if the missing data occurred consecutively. Finally, we required that each segment not contain a discontinuous jump, as this introduces artificial harmonics into the spectra. The relative amplitude of artificial harmonics in a spectral

estimate caused by a jump in the data series decreases as the total variation of the data series increases. Therefore our definition of a discontinuity relates the increase in density to the variance within the interval. We subtracted a third order polynomial fit from the data series and calculated the standard deviation of this detrended data series. Segments that contained changes in the five-point running average of the number density that exceeded 3.7 standard deviations, and that occurred within a 500 Mm window, were considered to contain discontinuities and were not analyzed. Since this discontinuity test depends on the variance of the entire data series, a density jump of a fixed amplitude that is considered a discontinuity in one segment may not be one in another segment that shares the same density jump. Our requirement that a spectral peak pass a phase coherence F-test additionally minimizes the inclusion of artificial peaks.

[7] We performed spectral analysis on each segment that passed all of the above criteria, fit the background spectra and performed two independent tests for spectral peak significance. For the data sampled at 35.4 Mm spatial resolution, we analyzed only segments that had a mean radial speed <550 km/s, and for the data sampled at 56.7 Mm we only analyzed segments that had a mean radial speed $\geq$550 km/s. The spectral analysis technique is based on multitaper windowing [*Thomson*, 1982], a robust autoregressive background fit, and a modified F-test [*Mann and Lees*, 1996]. The multitaper method of spectral analysis convolves multiple, orthogonal data tapers, in this case discrete prolate spheroidal sequences, with the segment of interest. This method reduces the variance of the spectral estimate and minimizes spectral leakage from the finite data series [*Ghil et al.*, 2002]. We require that a spectral peak pass both the F-test, which tests for phase coherent signals, and the narrow band test, which tests for significant power relative to the background spectral shape, at the 95% confidence levels. Solar wind number density spectra exhibit more power at longer wavelengths than at shorter wavelengths, a characteristic feature of a red noise spectrum, and can be modeled using the spectra of the first-order autoregressive, or AR(1), process. We use the method described by *Mann and Lees* [1996] for a robust background estimate of the spectra and assume an AR(1) spectra as the background.
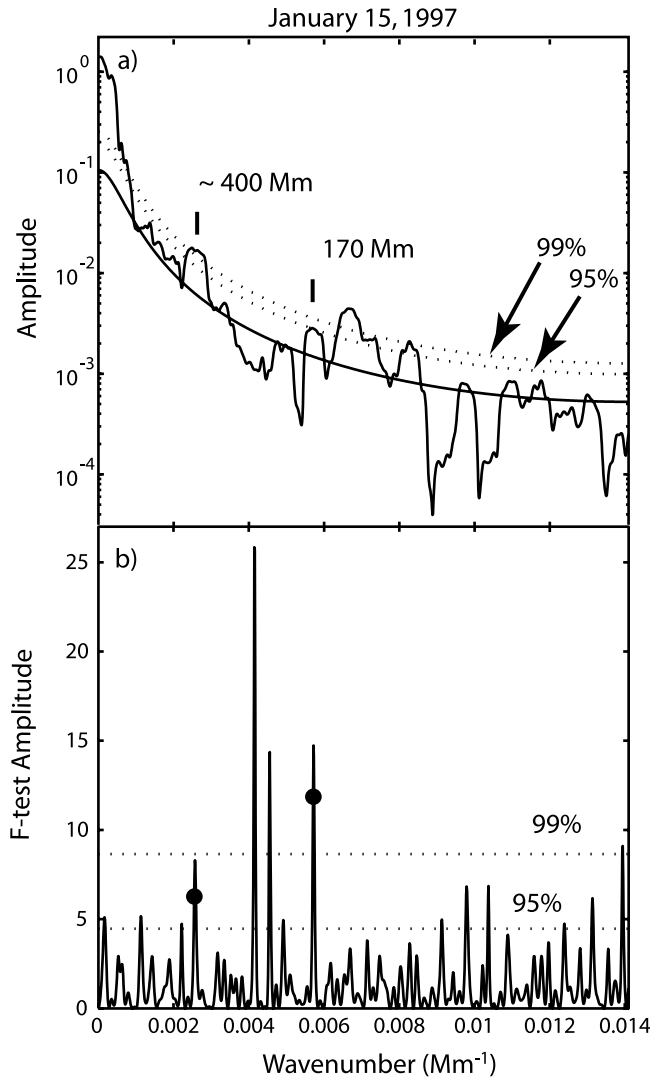
January 15, 1997

Figure 2. (a) Fourier amplitude spectra, autoregressive background fit (solid line) and narrow band amplitude test at the 95% and 99% significance levels (dashed lines). (b) Thomson's modified F-test for phase coherent signals (harmonic F-test) at the 95% and 99% significance levels. Two spectral peaks pass both tests simultaneously at the 95% level and are indicated with vertical ticks Figure 2a and dots Figure 2b.

[8] Figure 1 is an example of an event similar to those shown by *Kepko and Spence* [2003], showing an interval from 15 January 1997, when periodic number density structures were observed in the solar wind. In Figure 1, we show a 9072-Mm-long solar wind number density segment, measured by the Wind SWE instrument. Wind was located at (121, 28, 9) R_E in GSE coordinates. The x axis is given in length steps (35.4 Mm steps) measured from the beginning of the event. Tick marks show a clear ~400 Mm periodicity.

[9] Figure 2 illustrates an example of this spectral technique and two significance tests as applied to our analysis. The first step in the analysis of each segment was to estimate the spectra using Thomson's multitaper method

[*Thomson*, 1982]. The spectral estimate of the data series presented in Figure 1 is presented in Figure 2a with the AR(1) background fit (solid). We tested the spectral estimate for significant peaks using both a narrow band test (Figure 2a) and a harmonic F-test (Figure 2b) [*Thomson*, 1982]. The narrow band test requires that the residual spectrum at a given wave number have an amplitude that exceeds specified thresholds above the background spectral shape. For our analysis, we require amplitudes exceeding the 95% confidence level (lower dashed line in Figure 2a). For our example event, the following peaks pass the narrow band test at the 95% confidence level: $1/L = 2.6, 5.7, 6.5-7.5$, and 8.3×10^{-3} Mm^{-1} (Figure 2a). The harmonic F-test compares the variance from a pure sinusoid at wave number $1/L$ to the variance from the spectral estimate; large values of the F-test indicate that there is a true harmonic signal at $1/L$ in the interval. In this example, 13 wave numbers were significant at the 95% level (lower dashed line in Figure 2b). The upper dashed lines in Figures 2a and 2b are the 99% confidence level, shown for reference.

[10] It is possible for a signal to have low power and pass the F-test; it is also possible for a signal to have significant power and pass the narrow band test, but not pass the F-test. We therefore demand that a spectral peak pass both the narrow band test and the harmonic F-test simultaneously at the 95% confidence level to be counted as significant. Our requirement that wave numbers pass both tests simultaneously at the 95% level yields $1/L = 2.6$ and 5.7×10^{-3} Mm^{-1} (indicated with dashes in Figure 2a and dots in Figure 2b) as wave numbers that were counted in our statistics for this data segment. The 2.6×10^{-3} Mm^{-1} wave number has a wavelength of approximately 400 Mm, which is the wavelength we identified visually in Figure 1. Note that requiring both tests considerably reduces the number of peaks counted as compared to either test alone. A spectral enhancement that passes the amplitude test owing to an underestimation of the background will not pass the F-test unless it is a true harmonic signal. On the other hand, a false detection in the F-test with no power enhancement will not pass the narrow band test. In this way, we have minimized counting spurious spectral peaks, and rigorously kept only exceptionally significant spectral peaks.

[11] Once we identify the spectral peaks that pass our significance test, we calculate occurrence distributions by counting the number of statistically significant wave numbers found in a $6\Delta(1/L)$ wide band, shifting by $3\Delta(1/L)$ for each subsequent occurrence distribution point. We test for statistically significant occurrence enhancements in the occurrence distributions of the periodic radial length-scales found. The statistically significant periodic length-scales that we counted for each analyzed segment have at least two sources: apparently periodic solar wind fluctuations that occur intermittently even in a turbulent medium, and random statistically significant peaks that occur owing to the nature of statistics. These two sources by themselves would yield an occurrence distribution without enhancements at any particular length-scale. Significant enhancements in the occurrence distributions therefore imply the presence of recurrent physical phenomena.

[12] While the AR(1) spectra provides a close fit to the solar wind number density spectra, on average we find that it
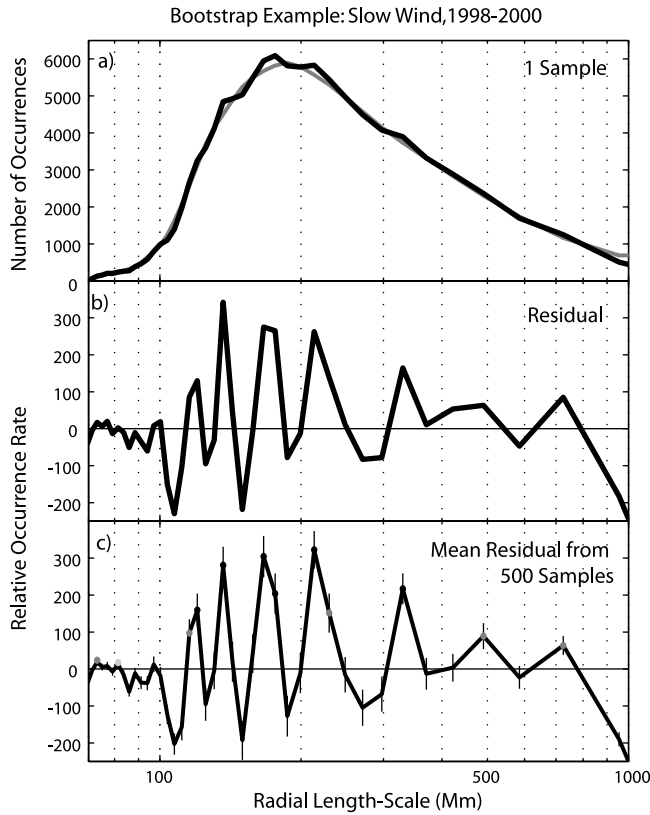
therefore minimize this artifact by subtracting a background occurrence distribution and examine only the residuals. Because we are interested in the relative occurrence of discrete spectral peaks in relation to the background occurrence distribution, this slight misfit does not affect our results.

[13] We use the bootstrap method to determine if enhancements in the occurrence distribution are statistically significant relative to the background. The bootstrap is a statistical method through which the uncertainty in a result can be estimated. In the bootstrap method, the uncertainty is estimated by repeating the analysis on a large number of random samples from the original data set [*Efron and Tibshirani*, 1993]. As discussed previously, we separate the results into slow and fast wind occurrence distributions. Next, we discuss our implementation of the bootstrap method to determine the uncertainty in the occurrence enhancements. We take 500 randomly generated bootstrap samples of the periodic radial length-scales that were found within each 3-year interval of time for the slow wind and the fast wind. For each bootstrap sample, we calculate a new occurrence distribution and fit this occurrence distribution with a (5-point) running average. We remove the background in order to determine the relative occurrence rate of statistically significant spectral peaks, and not the overall shape of the background, as the shape can be influenced by the spectral fit. Figure 3a shows an example of an occurrence distribution (black) generated from one bootstrap sample of the statistically significant radial wavelengths found for slow wind in 1998–2000, along with the background fit (grey). The residual of that occurrence distribution with the background subtracted is shown in Figure 3b. The *x* axis is plotted in radial length-scale (wavelength), and it is on a logarithmic scale. Note that as a result of the spectral analysis, the points in the occurrence distribution are spaced in equal $\Delta(1/L)$ steps, not equal ΔL steps; the distance between each discrete length-scale increases with increasing length-scale. For example, at L = 100 Mm the step size is approximately 3 Mm, while at L = 500 Mm, the step size is approximately 100 Mm.

[14] Localized peaks in the occurrence distribution indicate that certain length-scales occur more often than neighboring length-scales. For example, in this occurrence distribution statistically significant periodic length-scales near L = 136 Mm occur more often than neighboring length-scales. We take the mean value of the 500 residuals at each length-scale. If a majority of the bootstrap samples exhibit consistent occurrence enhancements, the result will be a mean residual that is greater than zero at those length-scales. We define the occurrence enhancement as statistically significant if the mean residual at that length-scale is at least one standard deviation above zero. Figure 3c shows the mean residual for the slow wind in the 1998–2000 interval, with a vertical line at each radial length-scale indicating ± one standard deviation. Statistically significant occurrence enhancements are marked with dots: light grey indicates that the length-scale was at least one standard deviation above zero, dark gray indicates that it was at least two standard deviations above zero, and black indicates that it was at least three standard deviations above zero. Note that the mean residual appears similar to the single bootstrap residual shown in Figure 3b, indicating that the results are

Figure 3. (a) Occurrence distribution from one bootstrap sample (black) taken from the slow wind distribution of statistically significant radial wavelengths found during 1998–2000 and the background fit (grey). (b) Residual of the occurrence distribution shown in Figure 3a with the fit removed. (c) Mean residual using 500 bootstrapped distributions. Vertical lines at each radial length-scale indicate ± one standard deviation of the residual at that length-scale. Dots mark statistically significant occurrence enhancements at one sigma (light grey), two sigma (dark grey), and three sigma (black) thresholds.

slightly underestimates the $1.1-9.8\,(2.8-7.7) \times 10^{-3}\,\mathrm{Mm}^{-1}$ range of the spectra for the 35.4 (56.7) Mm sampling rate and slightly overestimates the background of the spectral bands at larger and smaller wave numbers. This has the effect of artificially introducing a broad hump into the occurrence distribution of significant wave numbers near the center of the window, as peaks in this range systematically passed at a slightly lower significance threshold on the amplitude test than signals at the lower and higher wave numbers. However, this had no effect on the *F*-test. The occurrence distribution of peaks identified using just the *F*-test contains enhancements on top of a relatively flat background. One should be careful not to ascribe physical significance to the overall shape of the occurrence distribution; a different model for the background, or slightly different AR model parameters, would produce a different shape for the distribution. Because of the smoothly varying nature of the background and the fit, any slight differences between the model fit and the background would have trivial effects on the relative occurrence rate of neighboring wavelengths. We

Table 1. Statistics of the Analyzed Segments[a]

Year	Slow				Fast			
	Segments Analyzed		≥1 Significant Spectral Peak N		Segments Analyzed		≥1 Significant Spectral Peak	
	N	%	N	%	N	%	N	%
1995–1997	59677	42%	40248	67%	12674	9%	5554	44%
1996–1998	56660	41%	39389	70%	4562	3%	1976	42%
1997–1999	42005	31%	29950	71%	3051	2%	1542	51%
1998–2000	31716	22%	24492	77%	4840	3%	2640	55%
1999–2001	20396	14%	15953	78%	4393	3%	2364	54%
2000–2002	21987	15%	17470	79%	6702	5%	3914	58%
2001–2003	23558	15%	19340	82%	16063	10%	9778	61%
2002–2004	35238	22%	28744	82%	17441	11%	10568	61%
2003–2005	45302	28%	36656	81%	23417	14%	14517	62%

[a]The left two columns are for the slow wind, the right two are for the fast wind. The first (third) column shows the total number of all of segments that were analyzed for each year for the slow (fast) wind. The percent in the first (third) column is the percent of segments that met both our slow (or fast) restriction and the criteria discussed in the Methods section, out of all possible segments. Those numbers indicate how many segments we removed using the criteria discussed in the Methods section. The second (fourth) column shows the total number and percent of analyzed segments that contained at least one statistically significant spectral peak for the slow (fast) wind.

driven by good statistics. We find that during slow wind periods in 1998–2000, there are five occurrence enhancements at the three sigma threshold at L = 120, 136, 170, 220, and 330 Mm; at the two sigma threshold there are three additional occurrence enhancements at L = 73, 500, and 700 Mm; at the one sigma threshold there is one additional occurrence enhancement at L = 81 Mm.

3. Results

[15] We analyzed 11 years of solar wind number density data from Wind and recorded spectral peaks that simultaneously passed both the narrow band test and Thomson's modified F-test at the 95% confidence level, separating the slow and fast wind. The number of segments analyzed for the slow and fast wind, and the number of analyzed segments that contained at least one significant spectral peak between 72 Mm (the Nyquist wavelength) and 900 Mm for slow wind, and between 116 Mm and 900 Mm for fast wind, are listed in Table 1. The low number of segments analyzed for 1999–2002 is due to the Wind perigee passes, which we explicitly exclude from analysis.

[16] As described in section 2 and illustrated in Figure 3, we test for statistically significant enhancements in the occurrence distribution at three significance levels. Figure 4 shows the mean residuals computed for 3-year intervals of slow wind (Figure 4a) and fast wind (Figure 4b). The uncertainty (±one sigma) of the residual value at each length-scale is indicated with a vertical line. Occurrence enhancements are marked with light grey dots if they are at least one standard deviation above zero, dark grey if they are at least two standard deviations above zero, and black if they are at least three standard deviations above zero.

[17] There are particular radial length-scales that persist as occurrence enhancements throughout all 11 years of data within each speed range. For example, in the slow wind distributions (Figure 4a) there is a statistically significant occurrence enhancement centered near L = 136 Mm in all nine of the distributions. Also, there is an occurrence enhancement near L = 116 Mm that is at least one standard deviation above zero in eight of the nine distributions (1995–2004); even in the 2003–2005 distribution (top

there is a relative occurrence enhancement at L = 116 Mm, though it is not above the one sigma threshold. Some of the occurrence enhancement centers and widths appear to evolve slightly with time. For example, there is an occurrence enhancement centered near L = 176 Mm present in all nine of the distributions. Sometimes it encompasses an occurrence enhancement centered near L = 215 Mm, but sometimes it is a separate enhancement.

[18] For the fast wind distributions (Figure 4b), there are three length-scales quantified as statistically significant occurrence enhancements throughout most of the 11 years. There is a statistically significant occurrence enhancement near L = 187 Mm present in eight of the nine distributions. The other two length-scale occurrence enhancement centers and widths may evolve slightly, as appeared to occur in some of the slow wind occurrence enhancements. The occurrence enhancement near L = 400 Mm, present in seven of the distributions, encompasses 370 Mm in the 1996–1998 distribution, shifts slightly in 1998–2000 to encompass 500 Mm, and then returns in 2001–2003, encompassing 370 Mm. Similarly, the enhancement near L = 230 Mm evolves throughout the years, centered near 230 Mm in the 1995–1997 distribution, then near 270 Mm. The consistency between length-scale occurrence enhancements within each speed range of consecutive 3-year distributions gives additional confidence that the enhancements are not merely statistical variability.

4. Discussion

[19] The results presented in Figure 4 suggest that particular radial length-scales occur in periodic solar wind number density structures more often than would occur from random fluctuations, even at the > three sigma level. Some length-scale occurrence enhancements (for example, L = 136 Mm for slow wind and L = 187 Mm for fast wind) appear stable during the entire 11-year interval, while others evolve slowly (for example, L ∼ 180 Mm for slow wind and L ∼ 270 Mm for fast wind), perhaps due to a solar cycle dependence. The results suggest that certain sets of length-scales are inherent to periodic solar wind number density structures.
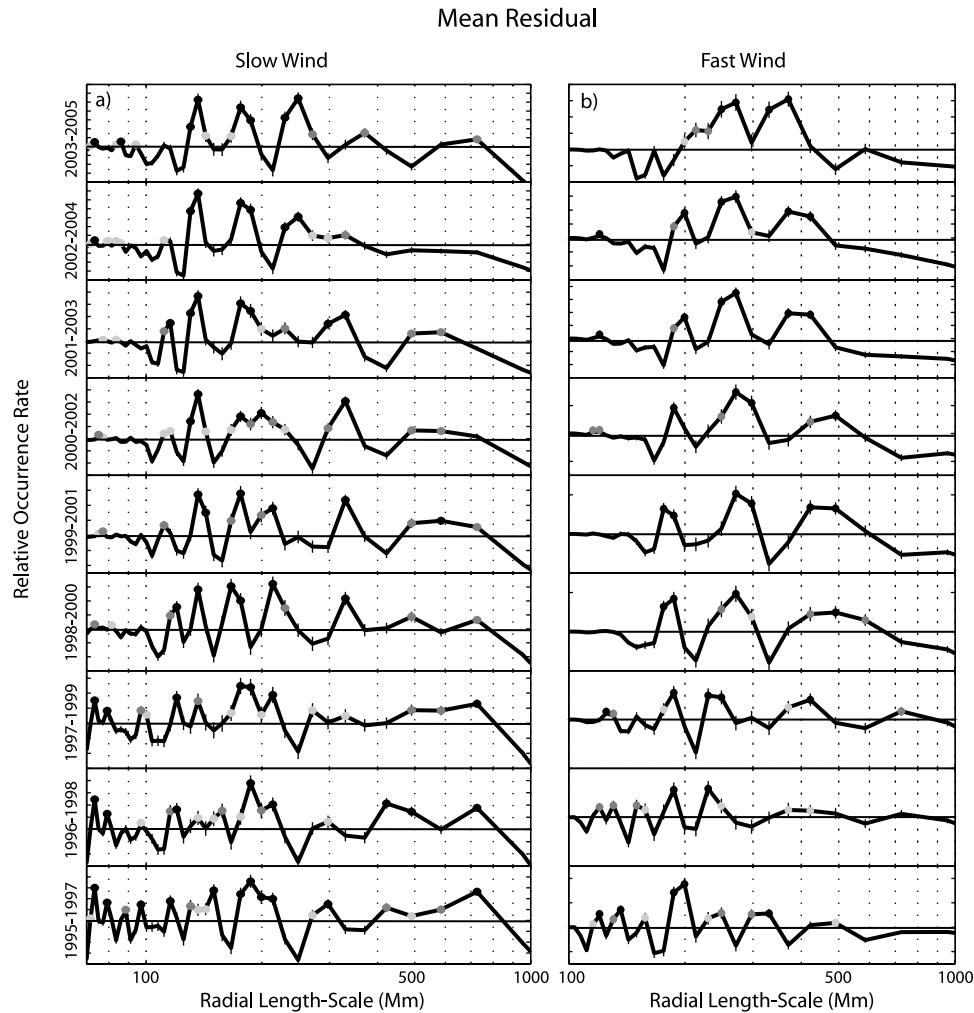
Mean Residual

Figure 4. Mean residuals of the 3-year radial length-scale occurrence distributions for (a) slow and (b) fast solar wind from 1995–2005. Vertical lines at each length-scale indicate ± one standard deviation of the residual at that length-scale, and dots indicate statistically significant occurrence enhancements at one sigma (light grey), two sigma (dark grey), and three sigma (black) thresholds. *Y* axis tick marks are every 100 occurrences.

[20] Figure 5 summarizes the values of the length-scale occurrence enhancements present at the three sigma level, calculated from our analysis of the slow (Figure 5a) and fast (Figure 5b) wind distributions. The bar below each value indicates the approximate width of the enhancement, determined by the number of length-scale points in each occurrence enhancement that are three standard deviations above zero. The value listed is the center of that portion of the occurrence enhancement. This figure highlights the consistency of the length-scale enhancements within each speed range for the 11 years studied here. Length-scale enhancements that are present for the majority of the slow wind distributions at the three sigma level are near L ∼ 73,120, 136, 180 Mm. Length-scale enhancements that are present for the majority of the fast wind distributions at the three sigma level are near L ∼ 187, 270, and 400 Mm. This list is conservative, as it includes only those enhancements with mean residuals at least three standard deviations above zero. Relative enhancements that fall below this threshold are not

included. For example, an occurrence enhancement near L ∼ 330 Mm is present in the majority of the slow wind distributions, however it is not included in our list, as it is only above the three sigma threshold in four of the distributions. Similarly, an occurrence enhancement near L ∼ 120 Mm is present in the majority of the fast wind distributions, but only at the two sigma threshold, so it is also excluded from our list. In our future work, it will be important to investigate the characteristics of these length-scales that are occurrence enhancements in a majority of the distributions at a lower significance threshold, as their persistence as occurrence enhancements suggests that they are also physically significant. Additionally, within a given distribution there are peaks that sometimes are close in length-scale that may physically be the same, though they are spectrally separate; for example L = 175 and 200 Mm for the 2000–2003 slow wind distribution. Note that the L = 180 Mm length-scale consistently observed in the slow wind is only one point in the occurrence distribution away
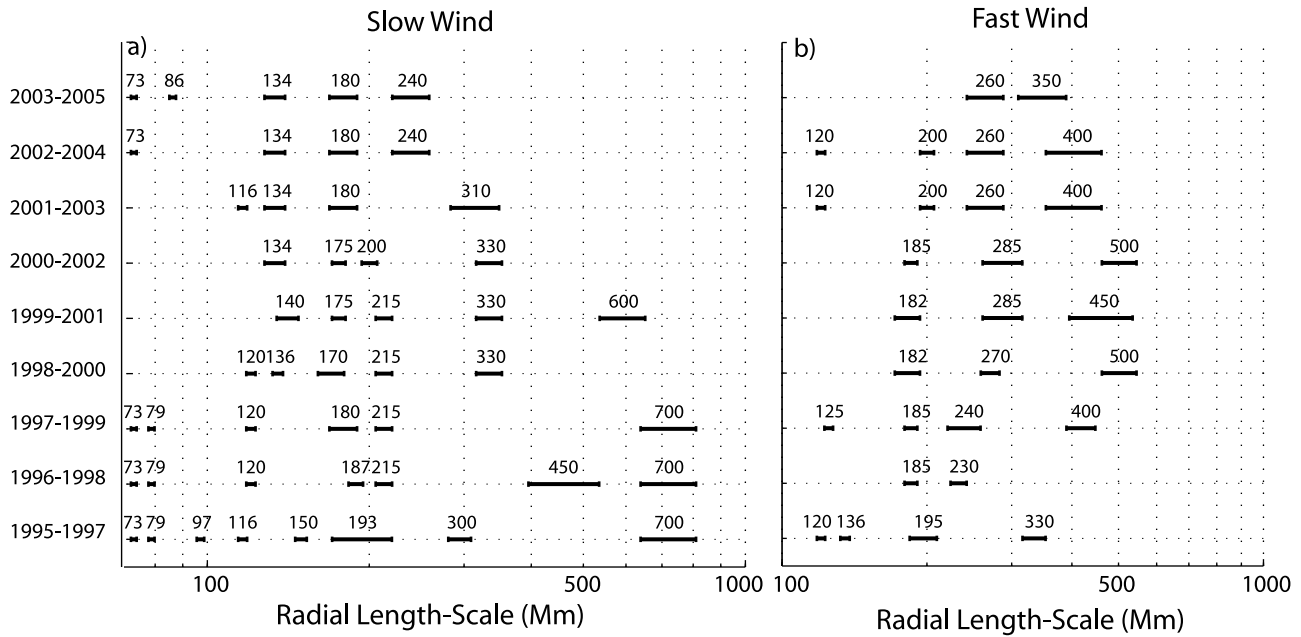
Figure 5. Summary of the occurrence distribution enhancements at the three sigma significance level shown in Figure 4. (a) Those identified in the slow wind occurrence distributions. (b) Those identified in the fast wind occurrence distributions. Bar width beneath each occurrence enhancement value represents the approximate width of the length-scale band enhancement.

from the L = 187 Mm length-scale that is consistently observed in the fast wind. As part of our future work, we will determine if the similar length-scales observed in the fast and slow wind results are due a common physical mechanism.

[21] It should be noted that the length-scales presented by *Kepko and Spence* [2003] and those that we have studied here are convecting periodic density structures and are fundamentally different from the correlation length-scale of the solar wind, which has been extensively studied [see, e.g., *Crooker et al.*, 1982; *Collier et al.*, 2000]. *Crooker et al.* [1982] found a characteristic correlation scale length of 20 R_E (130 Mm) perpendicular to the IMF during low IMF variance, and up to 50 R_E (320 Mm) during high variance. *Collier et al.* [2000] extended the analysis and demonstrated that the average radius of curvature of solar wind structures is about 100 R_E (640 Mm). These length-scales are similar in value to the periodic number density structure size scales. However, a connection between a correlation length-scale and the recurrent periodic length-scales studied in this paper is not obvious. *Bruno et al.* [2001] and *Borovsky* [2008] also presented evidence of underlying structure to the solar wind. Both papers suggested that the solar wind is not fully turbulent; rather there is underlying structure to the solar wind in the form of flux tubes that isolate different plasmas. *Borovsky* [2008] proposed that these flux tubes are "fossil structures", created near the solar surface and convecting outward into the heliosphere.

[22] While we established the existence of sets of particular radial length-scales in periodic solar wind number density structures, the physical mechanism creating these periodicities is unknown, and we can only speculate their cause. Examination of solar wind characteristics and their

variations during periodic solar wind number density structures may illuminate the underlying physical mechanism. Identifying where they occur relative to the heliospheric structure may also help to identify their source. Whether or not the structures are in pressure balance, and consequently undergo evolution as they convect outward in the heliosphere, is another important step in identifying their source. Additionally, turbulent mixing may process these structures as they convect with the solar wind. The slow solar wind is more turbulent and more intermittent than the fast solar wind [e.g., *Bruno and Carbone*, 2005], so any processing will likely be different in the two types of solar wind, possibly explaining some of the differences between the slow and fast wind results. We note that *Collier et al.* [2000] related the 100 R_E (640 Mm) correlation size scale they determined at 1 AU to the size scale of photospheric granular cells, which display a characteristic decay time of 5 min. *Ulrich* [1996] related this timescale to outward propagating Alfvén waves. A length-scale enhancement that was present for seven of the nine slow wind distributions was near 500 Mm and, if the source of these structures is the solar surface, this length-scale similarly maps back to characteristic photospheric granular cell dimensions. We note, however, that the length-scales studied here are radial, and a connection to perpendicular scale size on the solar surface is not immediately clear, though there are ideas involving magnetic reconnection wherein horizontal sizes directly translate into radial scales. Last, *Borovsky* [2008] related the time between flux tube wall crossings (Δt) observed at 1 AU to their mapped distance on the solar surface (Δx). Taking the equatorial solar surface velocity (1.87 km/s), *Borovsky* [2008] maps the flux tubes back to solar surface sizes using the following equation: $\Delta x = (1.87 \text{ km/s}) \Delta t$. The median

size scale that the flux tubes map to is 2.27 Mm, a typical granule size.

5.   Summary and Conclusion

[23]   While previous event studies have shown the existence of highly periodic number density variations in the solar wind [*Kepko et al.*, 2002; *Stephenson and Walker*, 2002; *Kepko and Spence*, 2003], they did not determine whether periodic density structures occur at particular radial wavelengths more often than at others. This paper presents the first statistical study of the relative occurrence rate of periodic solar wind number density structures. We performed a rigorous analysis of statistically significant radial wavelengths in 11 years of the solar wind number density data. We used the spectral analysis methods of *Thomson* [1982] and *Mann and Lees* [1996] to test for wavelength significance in 9072-Mm -long data segments and the bootstrap method to test for statistically significant occurrence enhancements in the occurrence distributions. We statistically demonstrate for the first time that particular length-scales are recurrent in periodic solar wind number density structures.

[24]   Our results are shown in Figure 5, which summarizes the radial length-scale occurrence enhancements present at the three sigma threshold, with the approximate enhancement width indicated by the bar beneath. Length-scale enhancements that are present for the majority of the slow wind distributions at the three sigma level are near L $\sim$ 73, 120, 136, and 180 Mm. Length-scale enhancements that are present for the majority of the fast wind distributions at the three sigma level are near L $\sim$ 187, 270, and 400 Mm.

[25]   There are reasons to speculate that the source of the periodic number density structures could be at the Sun. *Kepko and Spence* [2003] suggested a possible mechanism as being interchange reconnection modulated by solar oscillations. A possible connection is to kink oscillations in coronal loops, which have been observed by TRACE to have periods of 7–8 min [*Nakariakov and Verwichte*, 2004]. *Kepko and Spence* [2003] suggested that, in general, mechanisms that could vary reconnection on relevant time-scales could lead to periodic density variations in the solar wind. Further analysis and investigation will be necessary, and is underway, to establish the underlying source of periodic solar wind number density structures.

References

Borovsky, J. E. (2008), On the flux-tube texture of the solar wind: Strands of the magnetic carpet at 1 AU?, *J. Geophys. Res.*, doi:10.1029/2007JA012684, in press.

Bruno, R., and V. Carbone (2005), The solar wind as a turbulence laboratory, *J. Living Rev. Sol.*, 2, 5–134.

Bruno, R., V. Carbone, P. Veltri, E. Pietropaolo, and B. Bavassano (2001), Identifying intermittent events in the solar wind, *Planet. Space Sci.*, 49, 1201–1210.

Collier, M. R., A. Szabo, J. A. Slavin, and R. P. Lepping (2000), IMF length scales and predictability: The two length scale medium, *Int. J. Geomagn. Aeron.*, 2(1), 3–16.

Crooker, N. U., G. L. Siscoe, C. T. Russell, and E. J. Smith (1982), Factors controlling degree of correlation between ISEE 1 and ISEE 3 interplanetary magnetic field measurements, *J. Geophys. Res.*, 87(A4), 2224–2230.

Efron, B., and R. J. Tibshirani (1993), *An Introduction to the Bootstrap*, CRC Press, Boca Raton, Fla.

Ghil, M., et al. (2002), Advanced spectral methods for climatic time series, *Rev. Geophys.*, 40(1), 1003, doi:10.1029/2000RG000092.

Kepko, L., and H. E. Spence (2003), Observations of discrete, global magnetospheric oscillations directly driven by solar wind density variations, *J. Geophys. Res.*, 108(A6), 1257, doi:10.1029/2002JA009676.

Kepko, L., H. E. Spence, and H. J. Singer (2002), ULF waves in the solar wind as direct drivers of magnetospheric pulsations, *Geophys. Res. Lett.*, 29(8), 1197, doi:10.1029/2001GL014405.

Mann, M., and J. M. Lees (1996), Robust estimation of background noise and signal detection in climatic time series, *Clim. Change*, 33, 409–445.

Nakariakov, V. M., and E. Verwichte (2004), Seismology of the corona of the Sun, *Astron. Geophys.*, 45(4), 26–27.

Ogilvie, K. W., et al. (1995), SWE, a comprehensive plasma instrument for the Wind spacecraft, *Space Sci. Rev.*, 71, 55–77.

Stephenson, J. A. E., and A. D. M. Walker (2002), HF radar observations of Pc5 ULF pulsations driven by the solar wind, *Geophys. Res. Lett.*, 29(9), 1297, doi:10.1029/2001GL014291.

Thomson, D. J. (1982), Spectrum estimation and harmonic analysis, *IEEE Proc.*, 70, 1055–1096.

Ulrich, R. (1996), Observations of magnetohydrodynamic oscillations in the solar atmosphere with properties of Alfvén Waves, *Astrophys. J.*, 465, 436, doi:086/177431.

_____

L. Kepko, Space Science Center, University of New Hampshire, Morse Hall, Room 244, 39 College Road, Durham, NH 03824-3525, USA.

H. E. Spence and N. M. Viall, Center for Space Physics, Boston University, 725 Commonwealth Avenue, Boston, MA 2215, USA. (nickiv@bu.edu)